

# Bentonite pore distribution based on SAXS, chloride exclusion and NMR studies

A. MUURINEN<sup>1,\*</sup>, T. CARLSSON<sup>1</sup> AND A. ROOT<sup>2</sup>

<sup>1</sup> VTT Technical Research Centre of Finland, P.O. Box 1000, FI-02044 VTT, Finland, and  
<sup>2</sup> MagSol, Tuhkanummenkuja 2, 00970 Helsinki, Finland

(Received 4 December 2012; revised 18 March 2013; Editor: John Adams)

**ABSTRACT:** Water-saturated bentonite is planned to be used in many countries as an important barrier component in high-level nuclear waste (HLW) repositories. Knowledge about the microstructure of the bentonite and the distribution of water between interlayer (IL) and non-interlayer (non-IL) pores is important for modelling of long-term processes. In this work the microstructure of water-saturated samples prepared from MX-80 bentonite was studied with nuclear magnetic resonance (NMR) and small-angle X-ray scattering spectroscopy (SAXS) coupled with chloride exclusion modelling. The sample dry densities ranged between 0.7 and 1.6 g/cm<sup>3</sup>. The NMR technique was used to get information about the relative amounts of different water types. Water in smaller volume domains has a shorter relaxation time than that in larger domains due to the average closer proximity of the water to the paramagnetic Fe at the layer surfaces. The results were obtained using <sup>1</sup>H NMR  $T_{1\rho}$  relaxation time measurements with the short inter-pulse CPMG method. The interpretation of the NMR results was made by fitting a sum of discrete exponentials to the observed decay curves. The SAXS measurement on bentonite samples was used to get information about the size distribution of the IL distance of montmorillonite. The chloride porosity measurements and Donnan exclusion calculations were used together with the SAXS results to evaluate the bentonite microstructure. In the model, the montmorillonite layers were organized in stacks having IL water between the layers and non-IL water between the stacks. In the modelling, the number of layers in the stacks was used as fitting parameters which determined the IL and non-IL surface areas. The fitting parameters were adjusted so that the modelled chloride concentration was equal to the measured one. The NMR studies and SAXS studies coupled with the Cl porosity measurements provided very similar pictures of how the porewater is divided in two phases in bentonite.

**KEYWORDS:** high-level nuclear waste (HLW) repositories, bentonite buffer, microstructure, pore distribution, NMR, SAXS, exclusion.

Many of the performance targets of the KBS-3 concept are coupled to processes that occur in water-saturated bentonite. Examples of such processes are the swelling of bentonite, dissolution and precipitation phenomena and transport of water, colloids and ions through the clay. These processes are strongly coupled to how the water is distributed

between different pores in the bentonite microstructure. The material used in this study was MX-80 sodium bentonite from Wyoming, USA. The major component of the bentonite is montmorillonite, which confers its swelling properties and essential microstructural features. Details about the MX-80 bentonite composition are found in Karnland *et al.* (2006).

The central structural unit of the montmorillonite is the negatively charged tetrahedral-octahedral-tetrahedral layer constructed of silica, aluminium and oxygen atoms. Details concerning the structure

\* E-mail: arto.muurinen@vtt.fi

DOI: 10.1180/claymin.2013.048.2.07

of the layer are presented elsewhere (e.g. van Olphen, 1977) and will not be repeated here. The diameter of the montmorillonite unit layer has been estimated to be 50–200 nm (Tournassat & Appelo, 2011, and references therein). The thickness of the montmorillonite unit layer varies between 0.92 and 1.01 nm (Holmboe *et al.*, 2012) and the montmorillonite surface area is 749 m<sup>2</sup>/g (Montavon *et al.*, 2009; Tournassat & Appelo, 2011). In bentonite, the surface area is less and can be evaluated on the basis of the montmorillonite content.

The literature contains an abundance of models that describe the microstructure of water-saturated bentonite and montmorillonite. The models differ in detail, but have a few features in common, like the montmorillonite unit layer, stacks, interlayer (IL) and non-interlayer (non-IL) pores/porewater. Recent results by Kaufhold *et al.* (2010) suggest that the ratio of non-IL water to IL water is coupled to the microstructure (porosity) of the bentonite. A brief overview of existing structure models is achieved by consulting Cebula *et al.* (1979), Pusch *et al.* (1990), Pusch (1999), Bradbury & Bayens (2003), Wersin (2003), Suzuki *et al.* (2004), Muurinen *et al.* (2007) and Tournassat & Appelo (2011). In contrast to the dual porosity suggested above, some microstructural models divide the non-IL water further into inter-particle and inter-aggregate pores. A wholly different opinion is presented by Birgersson & Karnland (2009) who claim that all water would be homogeneously distributed as interlayer water.

The objective of the present study was to determine the distribution of water in water-saturated Wyoming MX-80 bentonite by using NMR, SAXS and CI exclusion techniques. The amounts of IL and non-IL water presented in this report are coupled to the bentonite type and the experimental conditions, i.e. to the bentonite dry density and to the type and concentration of dissolved electrolyte in the porewater, etc. Thus, changing the porewater chemistry, other things being equal, might result in IL and non-IL water contents that differ considerably from the results of this study. NMR has previously been used successfully to determine the distribution of pore water in water-saturated bentonite and montmorillonite by, e.g. Montavon *et al.* (2009) and Ohkubo *et al.* (2008). The study by Montavon *et al.* was made on water-saturated compacted clay samples (illite, montmorillonite and MX-80 bento-

nite) by low-field proton NMR. By considering the differences in observed proton mobilities, it was possible to distinguish between three different populations – structural OH, external surface water, and internal surface water. The problem of rapid exchange between external surface water and bulk water in water-saturated clay was solved by freezing samples to –25°C. At this temperature, the bulk water was frozen, and therefore distinguishable from the surface water, which was in a semi-liquid state. The number of unfrozen water layers was about three, which is about the same as usually found in the literature. Ohkubo *et al.* (2008) used <sup>1</sup>H NMR *T*<sub>1</sub> relaxation in a study of water in water-saturated compacted bentonites – Kunipia-F (a purified bentonite with a montmorillonite content >98 wt.%) and Kunigel-V1 (crude material with a montmorillonite content of 59.3 wt.%). The *T*<sub>1</sub> relaxation decay signals in the NMR measurements were considered to contain contributions from several relaxation processes in the sample, and mathematical analyses of the exponential decays indicated the presence of several relaxation mechanisms. Based on this, Ohkubo *et al.* were, among other things, able to estimate the ratio of bulk-like water to total water. The term ‘bulk-like water’ corresponds to what is here referred to as ‘non-IL water’, i.e. the results by Ohkubo *et al.* show the usefulness of NMR as a tool for determining the relative amounts of IL and non-IL water in materials such as water-saturated bentonite.

XRD and SAXS are well established techniques for studying the changes in the interlayer distances in bentonite and montmorillonite. XRD and SAXS measurements do not always give a 001 peak that can be interpreted in terms of a single IL distance. Samples containing mixed-layer structures have their total IL space made up of sub-spaces, each one being characterized by a discrete number (0, 1, 2, ...) of IL water layers. Peak profile modelling can in this case be used to estimate the respective contributions of various mixed-layer structures to the observed peaks. Peak profile modelling has been successfully applied to dilute montmorillonite solutions or suspensions (Ferrage *et al.*, 2005; Tertre *et al.*, 2011a,b) and in compacted MX-80 bentonite (Holmboe *et al.*, 2012). The latter reference claims that the basal spacing obtained from Bragg’s law may differ by as much as 1 Å from the basal spacing concluded from XRD profile fitting. However, fig. 12 in Holmboe *et al.* offers an alternative interpretation as well; irrespective of

whether Bragg's law or profile modelling is used, the same result is obtained, with an uncertainty of  $\pm 1$  Å.

Morvan *et al.* (1994) used ultrasmall- and small-angle X-ray scattering for studies of the microstructure of sodium montmorillonite suspensions in deionized water. The observed interlayer distances were smaller than the ideal ones, indicating that the montmorillonite sheets cannot be uniformly dispersed in the whole sample. For example, the ideal and complete swelling for a 20% (w/w) sodium montmorillonite suspension would be 105 Å. Experimentally the peak was observed at 56 Å, which means that half of the water did not participate in the swelling process and was present in excess domains. SAXS measurements by Segad *et al.* (2010) indicate that the simple picture of clay consisting of well organized platelets in a perfect lamellar structure is incomplete. This conclusion was based on measurements of Ca montmorillonite having a clay/water ratio corresponding to an average interlayer water thickness of 100 Å. However, the thickness measured by SAXS was only  $\sim 10$  Å. The discrepancy could be explained by the formation of stacks containing a small number of montmorillonite unit layers. The number of the platelets was evaluated from the scattering peak width to be 10–20 which means that the separation between the stacks was 500–1000 Å. The conclusion by Segad *et al.* (2010) was that the swelling in the Ca montmorillonite took place between the stacks and not between single unit layers.

Warr & Berger (2007) used XRD to study the hydration behaviour of compacted Na-activated IBECO-SEAL-80 and Ca-activated TIXOTON-TE in a disc-shaped flow-through cell. The density of the IBECO-seal samples was about  $1.15 \text{ g/cm}^3$  and that of TIXOTON-TE samples  $0.94 \text{ g/cm}^3$ . Seawater and groundwater of low ionic strength were used for saturation of the samples. The amount of the IL water was calculated from the XRD patterns using the CALCMIX software. Subtraction of the IL water from the measured total water yielded the volume of the non-IL water. Roughly equal quantities of IL and non-IL water entered the Na-bentonite, whereas in the Ca-bentonite the non-IL and IL water contents were 77% and 23%, respectively.

Holmboe (2011) and Holmboe *et al.* (2012) used XRD in reflection mode to study the average basal distances of Wyoming bentonite MX-80 and the

corresponding homo-ionic Na- and Ca-montmorillonites as a function of water content. For compacted samples representative of the bentonite barrier in a deep geological repository, the interlayer distances obtained were compared against the corresponding theoretical maximum interlayer distances in order to calculate the free porosity. At a dry density of  $>1.4 \text{ g/cm}^3$  the average free porosity was calculated by Holmboe *et al.* to be  $<3\%$  for MX-80 and the corresponding homo-ionic Na-montmorillonite, which is significantly lower than that found in the literature.

The accessible porosity for anions in bentonite is smaller than the total porosity due to anion repulsion (exclusion) by the surface of montmorillonite. The accessible porosity is a function of the bentonite density and the salt concentration. Anion exclusion is well known in soil science and the Gouy-Chapman theory for the diffuse double layer has been applied to model anion exclusion in clay suspensions, for example in Bolt & Warkentin (1958), Edwards & Quirk (1962) and Bolt & De Haan (1982). Sposito (1982) improved the Gouy-Chapman model by adding the distance of minimal approach due to the ion size. Birgersson & Karland (2009) used the Donnan equation to calculate the exclusion in compacted bentonite in contact with an external NaCl solution assuming a uniform porosity in the bentonite. In Muurinen *et al.* (2007) and Muurinen (2009) the Donnan model was used for the experiments with compacted bentonite assuming two different pore types in bentonite. The anion exclusion has also been observed in many diffusion experiments performed in compacted bentonite (Eriksen & Jacobsson, 1984; Muurinen, 1994; Kozaki *et al.*, 2001; Moleira *et al.*, 2003; and Van Loon *et al.*, 2007). In Tournassat & Appelo (2011), anion exclusion data were gathered from the literature, reprocessed and modelled using different models. It was concluded that a heterogeneous pore distribution model reproduces the data better than a homogeneous one over a wide range of conditions. The number of layers in the stacks is a variable that remains to be related to sample preparation and experimental conditions.

The following presents a few simple formulae that facilitate discussions of how pore water is distributed in water-saturated montmorillonite. For convenience, the montmorillonite unit layers are assumed to be equally sized, have a thickness of about 1 nm, and lateral dimensions in the range

given above. Under these conditions, the area of the edges is negligible and all surfaces can be assumed to consist of the basal surfaces of the montmorillonite unit layer. Figure 1A describes a situation where all unit layers are uniformly distributed in a parallel manner and separated from each other by a maximum interlayer distance,  $t_{\max}$ . In this case, the total water content in the sample,  $V_{\text{tot}}$ , can be expressed as (Karnland *et al.*, 2005):

$$V_{\text{tot}} = \frac{S_{\text{tot}}}{2} t_{\max} \quad (1)$$

where  $S_{\text{tot}}$  is the total montmorillonite surface area in the sample. If the actual IL distance,  $t_{\text{av}}$ , is smaller than  $t_{\max}$ , then the water phase will be divided into two phases, IL and non-IL water. Sub-division of the non-IL water into, e.g. edge water, external double layer water, and free water, is possible but not necessary for the present discussion.

The distribution of water can be discussed in terms of stacks consisting of identical unit layers arranged in a parallel manner, see Fig. 1B and C. The volume of the IL water,  $V_{\text{IL}}$ , can then be written as:

$$V_{\text{IL}} = \frac{n-1}{n} \frac{S_{\text{tot}}}{2} t_{\text{av}} \quad (2)$$

where  $n$  is the stacking number, i.e. the number of unit layers in each stack. Equation 2 shows explicitly that the volume of the IL water is coupled to the number  $n$ , which has previously been pointed out by van Olphen (1977), Suzuki *et*

*al.* (2004) and Tournassat & Appelo (2011). According to equation 2, it is not possible to unambiguously determine  $V_{\text{IL}}$  from knowledge of  $S_{\text{tot}}$  and  $t_{\text{av}}$  alone; for given values of  $S_{\text{tot}}$  and  $t_{\text{av}}$ , different  $n$  values produces different  $V_{\text{IL}}$  values, see Fig. 1.

Combining equations 1 and 2 yields a relation between the volumes of IL water and total water:

$$V_{\text{IL}} = \frac{n-1}{n} \frac{t_{\text{av}}}{t_{\max}} V_{\text{tot}} \quad (3)$$

Thus, the volume of the IL water is clearly coupled to the stacking number. This is schematically demonstrated in Fig. 1. The first case (Fig. 1A) shows an ideal situation where all unit layers are equally distributed in a single water phase and separated by a maximum (theoretical) interlayer distance,  $t_{\max}$ . Figure 1B and C shows samples with the same number of layers and water as in A, containing randomly distributed stacks consisting of six or four unit layers, respectively. The layers are separated by an interlayer distance  $t_{\text{av}} < t_{\max}$ . Cases B and C are associated with the same surface area and the same interlayer distance, but their corresponding volumes of IL and non-IL water differ as a result of their different stacking numbers.

Dividing both sides of equation 3 by  $t_{\text{av}}$  yields the corresponding relation between the IL surface,  $S_{\text{IL}}$  and the total surface,  $S_{\text{tot}}$ :

$$S_{\text{IL}} = \frac{n-1}{n} S_{\text{tot}} \quad (4)$$

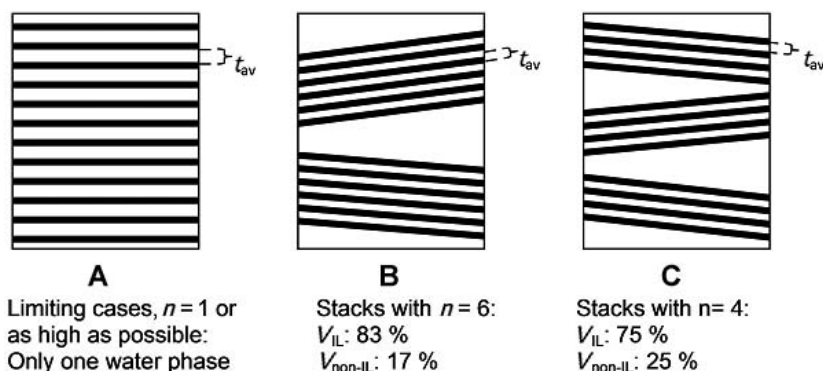


FIG. 1. Schematic illustration of the effect of stack formation in compacted water-saturated montmorillonite and the concomitant splitting of porewater into interlayer (IL) and non-interlayer (non-IL) water. The number of unit layers inside the stacks,  $n$ , strongly influences the IL and non-IL surface areas and volumes of IL and non-IL water.

where  $S_{IL} = 2V_{IL}/t_{av}$  and the other symbols have the same meaning as before. In order to be physically meaningful,  $n$  can only take values between two certain limits. The lower and the upper limits given by  $n = 1$  or  $n = n_{max}$ , where  $n_{max}$  is the highest possible number of unit layers in a given sample, are associated with a presence of only one water phase, see Fig. 1A.

When  $(n-1)/n$  is close to unity, equation 3 can be approximated by:

$$V_{IL} = \frac{t_{av}}{t_{max}} V_{tot} \tag{5}$$

This equation was used also by Holmboe *et al.* (2012) in their calculations. The conclusion from this deserves to be explicitly expressed; the application of equation 5 to water-saturated swelling clay containing individual stacks overestimates  $V_{IL}$  at the same time as it underestimates  $V_{non-IL}$ .

The volume of the non-IL water,  $V_{non-IL}$ , is the difference between the volumes of total water,  $V_{tot}$ , and the IL water,  $V_{IL}$ , which can be expressed as:

$$V_{non-IL} = V_{tot} \left( 1 - \frac{n-1}{n} \frac{t_{av}}{t_{max}} \right) \tag{6}$$

Equations 3 and 5 indicate that the relative proportions of IL and non-IL water in bentonite or a pure swelling clay cannot be evaluated by only determining the interlayer distances  $t_{av}$  and  $t_{max}$ . It is necessary to evaluate either  $S_{IL}$  and  $S_{non-IL}$  or  $V_{IL}$  and  $V_{non-IL}$ , too. In the present paper  $S_{IL}$  and  $S_{non-IL}$  were evaluated from exclusion calculations and  $V_{IL}$  and  $V_{non-IL}$  from NMR measurements.

The above relations concern pure montmorillonite. In case of MX-80 bentonite, only a fraction,  $\beta$ , is montmorillonite, while the remaining fraction,  $1-\beta$ , mainly consists of accessory minerals, see Karnland *et al.* (2006) for details. Since montmorillonite is the dominating mineral in MX-80 and the surface areas of the accessory minerals are negligible, the total surface of the MX-80,  $S_{tot,MX-80}$ , can then be approximated by

$$S_{tot,MX-80} = \beta S_{tot} \tag{7}$$

where  $S_{tot}$  is the total surface area of the montmorillonite. The value of  $t_{max}$  in the bentonite will then increase by a factor of  $1/\beta$ . For details concerning the effects of  $\beta$ , see Holmboe *et al.* (2012).

## EXPERIMENTAL

### Sample preparation

In the preparation of the samples, weighed amounts of MX-80 and Milli-Q water were mixed in proportions that corresponded to water-saturated MX-80 samples with target dry densities in the range 0.7–1.6 g/cm<sup>3</sup>. Each MX-80/water mixture was subsequently placed in a squeezing cell with an inner diameter of 20 mm and compacted. The squeezing cell was equipped with tubing that allowed air removal during compaction. Details concerning the squeezing cell are found in Muurinen & Carlsson (2010). After compaction, each sample was removed from the squeezing cell and transferred to a sample holder that formed the central part of a so-called equilibrium cell (Fig. 2). The sample holder consisted of a stainless steel plate with a hole that fitted the dimensions of the compacted sample.

The contact between the clay and the external solution took place via filter plates (from Applied Porous Technologies, Inc., Sweden). The filter plates (sinters) consisted of stainless steel discs with a diameter of 24.0 mm, a thickness of 1.24 mm and a pore diameter of 2 μm. The target dry densities of the samples were 0.7, 1.0, 1.3 and 1.6 g/cm<sup>3</sup>. The samples in the equilibrium cells were 9.5 mm in length and 20 mm in diameter. Somewhat different experimental arrangements and times were used in the NMR and SAXS experiments (see below). The compacted MX-80 bentonite samples were equilibrated with 0.1 M NaCl solution. The samples for NMR experiment were equilibrated for 7 to 33 days. The bentonites for the SAXS experiment were equilibrated for 12.5 months from only one end, i.e. the equilibration took place in cells having only one compartment with equilibrium solution. All the experiments were performed under aerobic conditions. Further details are found in Muurinen & Carlsson (2013).

### NMR experiment

Each equilibration cell was opened after a certain time (see below) and a sub-sample was put into a glass tube, which was sealed with Teflon stoppers and used in subsequent NMR measurement. The diameter and length of the sub-sample were 4.5 and 9.5 mm, respectively.

The measurements were carried out with a high-field Chemagnetics CMX Infinity 270 MHz NMR

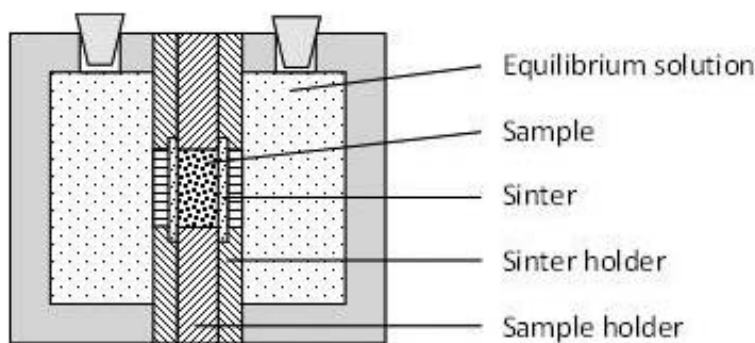


FIG. 2. Schematic drawing of an equilibrium cell. The sample is kept in a 9.5 mm thick stainless steel plate and stays in contact with an equilibrium solution *via* stainless steel sinters.

spectrometer using a spin-locking CPMG (Carr-Purcell-Meiboom-Gill) technique (Santyr *et al.*, 1988). Briefly, this means that measured signal decays are associated with the rotating-frame spin-lattice relaxation time,  $T_{1\rho}$  (e.g. Farrar & Becker 1971). This was confirmed by carrying out equivalent traditional  $T_{1\rho}$  experiments on some samples to check that the same signal decay was obtained. The use of the CPMG method to measure  $T_{1\rho}$  is advantageous, since the whole decay signal can be obtained in one shot and a finer resolution of the decay can be obtained for a given time. It is possible that  $T_{1\rho}$  and  $T_2$  are equivalent here, but it is unlikely  $T_2$  is measured with such a short refocusing delay (22  $\mu$ s). The measurement of  $T_{1\rho}$  necessitates that all CPMG measurements are carried out with the same inter-pulse spacing  $\tau$  in order to allow proper comparisons (same spin locking field) between results from different samples (Carlsson *et al.*, 2012, and references therein). To conclude, this study utilised  $^1\text{H}$  NMR  $T_{1\rho}$  relaxation time measurements using the short inter-pulse CPMG method. The time used between the centre of the  $180^\circ$  pulses,  $\tau$ , was 22  $\mu$ s in all cases (equivalent to a 22.7 kHz spin locking field). The software peak-o-mat (Kristukat, 2008) was used to fit discrete exponentials to the decay curves obtained from the NMR measurements. The sample temperature was kept at 23°C by gas flushing.

The determination of the relative amounts of different water types in water-saturated clay samples was made by a method similar to the one described by Ohkubo *et al.* (2008). Briefly, this means that in case several decays occur in the sample, the observed overall decay is given as:

$$M = \sum_1^n M_{0,i} \exp \left[ \frac{-t}{T_{1\rho,i}} \right] \quad (8)$$

where  $M$  is the spin locked macroscopic magnetization vector,  $t$  is time,  $M_{0,i}$  and  $T_{1\rho,i}$  are the zero time magnetization and the spin-lattice relaxation time in the rotating frame, respectively, associated with decay  $i$ . It was found in this study that the observed relaxation was composed of two major relaxation processes, which together comprised about 99% of the magnetization. Since water in smaller pores interacts more with paramagnetic  $\text{Fe}^{3+}$  than that in larger pores, the decay with the shorter relaxation time was associated with the IL water and the decay with the longer relaxation time with the non-IL water. It should be stressed that it is not *a priori* possible to tell how many relaxation processes are needed to fit the observed curve. In the present study, however, it was found that assuming a third relaxation process only had a marginal effect, which strongly suggests the presence of only two water phases.

#### SAXS experiment

At the end of the equilibration of the SAXS experiment the external solution was removed and its pH values measured. Later, the solution was filtered with 12 k MWCO ultrafilter and  $\text{Na}^+$ ,  $\text{K}^+$ ,  $\text{Ca}^{2+}$ ,  $\text{Mg}^{2+}$ ,  $\text{Cl}^-$ ,  $\text{SO}_4^{2-}$  and  $\text{HCO}_3^-$  were analysed. When the bentonites of the SAXS experiments were removed from the sample cell, a layer of 1 mm next to the filter plate, where the water content is often increased, was first removed. Half of the next layer

of 2 mm was used for the water content measurement by drying the sample two days at 105°C. The other half of the layer was used for determination of chloride concentration in the clay. The chloride analysis was performed by dispersing the bentonite sample of 0.3–1 g in 20 ml of deionized water. The samples were shaken for four days and then the solution was separated from the bentonite in a centrifuge. The solution was ultrafiltered with 12 k MWCO filter and chloride analysed with ion chromatography.

Small-angle X-ray Scattering (SAXS) measurements were performed on the rest of the bentonite sample. The measurements were carried out with a SAXS device consisting of a Bruker MICROSTAR microfocus rotating anode X-ray source with Montel Optics (parallel beam, Cu- $K\alpha$  radiation,  $\lambda = 1.54 \text{ \AA}$ ), where the beam was further collimated using three sets of JJ X-ray 4-blade slits. Two sample-to-detector distances were used in order to span different  $q$  ranges. The scattering intensities were measured using a 2D area detector (Bruker HiStar or Bruker Vântec). The magnitude of the scattering vector is given by  $q = (4\pi/\lambda)\sin\theta$ , where  $2\theta$  is the scattering angle. The dependence between the size ( $d$ ) of the structure causing scattering and the scattering vector ( $q$ ) is given by  $d = 2\pi/q$ . The  $q$  values were calibrated using a silver behenate standard ( $d = 58.4 \text{ \AA}$ ). Corrections for spatial distortion and detector response were made using a Fe-55 source. The SAXS patterns from the samples were absorption-corrected and the background scattering was subtracted. For SAXS measurement, the samples were cut into 0.5 mm-thick slices to keep the absorption of the direct X-ray beam at a reasonable level. Mylar foils were placed on each surface of the bentonite to prevent water content changes of the sample during the measurement.

## RESULTS AND DISCUSSION

### NMR results

The NMR measurements on water-saturated MX-80 bentonite samples yielded decay curves, which could be expressed as a sum of two exponential decays, see Fig. 3. Each decay curve  $i$  was associated with a zero time magnetization  $M_{0,i}$  and a corresponding spin-lattice relaxation time  $T_{1\rho,i}$ , as described by equation 8. The value of  $M_{0,i}$  was interpreted as a measure of the amount of water phase associated with the curve, while the two  $T_{1\rho}$

relaxation times were used to distinguish between two categories of porewater: IL water and non-IL water. As stated above, it could not *a priori* be expected that only two exponential decay curves would suffice to describe the observed relaxation time, but this was found to be the case for the samples investigated in this study. The results in Table 1 provide support for the idea that two, and only two, major types of porewater were present in the samples. This is seen in the column with  $M_{0,i}$  values that were achieved by assuming the presence of three porewater phases. The third  $M_{0,i}$  value was only about 1% of the total magnetization, which suggests that the possibility of a third water phase in the samples studied is negligible for the present purposes. Further examination of the data indicates that the  $T_{1\rho}$  relaxation times decrease with increasing dry density, or in other words, with decreasing water content. A reasonable explanation for this is found by realising that an increase in dry density reduces the pore volume and increases the clay surface area. This means that the porewater experiences a stronger influence from paramagnetic impurities in the montmorillonite structure, which is manifested by the shorter relaxation times shown. Inspection of Table 1 also shows a clear trend in how the  $M_0$  values vary with dry density:  $M_0$  values associated with the faster decays (shorter  $T_{1\rho}$  values), increase with increasing dry density, and *vice versa*; the  $M_0$  values associated with the slower

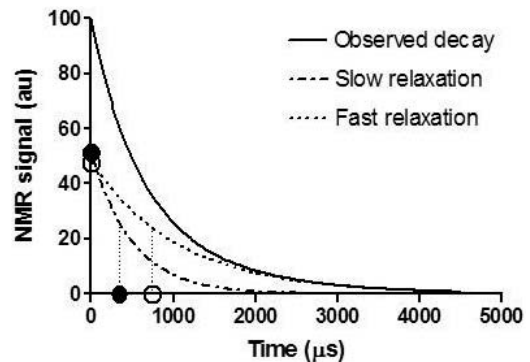


FIG. 3. Typical result from the NMR measurements on water-saturated MX-80 bentonite showing an observed decay curve (solid line), which could be split into two exponential functions (dotted lines), each one associated with a different relaxation time. The data points show zero time magnetization on the y axis and  $T_{1\rho}$  relaxation times on the x axis. Filled and open circles refer to fast and slow relaxation, respectively.

TABLE 1. Estimated fractions of IL water and non-IL water in 'as delivered' MX-80 bentonite determined from curve-fitting analysis. The fractions are given in per cent of the total porewater volume. The porosity,  $p$ , was calculated from the equation  $p = 1 - \rho_{\text{dry}}/\rho_{\text{g}}$ . The value of  $\rho_{\text{g}}$  used in the calculation was  $2.75 \text{ g/cm}^3$ .

Sample	External solution	Time (d)	Dry density ( $\text{g/cm}^3$ )	Porosity	Decay no., $i$	$T_{1\rho}$ ( $\mu\text{s}$ )	$M_{0,i}^{**}$	IL water (%)	Non-IL water (%)
MX-80	0.1 M NaCl	7	0.71	0.74	1	467	35.8	36	–
					2	1213	63.4	–	64
					3	16210	0.8	–	–
MX-80	0.1 M NaCl	15	0.96	0.65	1	341	51.2	52	–
					2	744	47.6	–	48
					3	20106	0.9	–	–
MX-80	0.1 M NaCl	24	1.27	0.54	1	286	63.1	63	–
					2	590	35.7	–	37
					3	21667	1.2	–	–
MX-80	0.1 M NaCl	33	1.57	0.43	1	189	66.7	67	–
					2	390	32.5	–	33
					3	24497	0.8	–	–

decays (longer  $T_{1\rho}$  values), decrease with increasing dry density.

Graphs of the type shown in Fig. 3 were observed for the MX-80 samples containing porewater, but not for the oven-dried MX-80. Measurements on oven-dried (105°C for 24 h) samples only produced small, insignificant signals emanating from protons in, e.g. structural OH groups within the structure of the montmorillonite unit layer. In other words, the results from the NMR measurements suggest that the two curves (Fig. 3) are associated with two distinguishable water phases located in two different types of pores. A reasonable distinction can tentatively be made in terms of the IL and non-IL water phases, an approach frequently found in the literature, see e.g. Pusch *et al.* (1990), Muurinen (1994), Wersin (2003), Suzuki *et al.* (2004), Fernández & Rivas (2005) and Warr & Berger (2007).

In order to couple the paired  $T_{1\rho}$  and  $M_0$  values with the proper water phase (IL or non-IL water), supporting data from the SAXS measurements below were used. The data of interest in this context were the determined volume fractions of the IL-porosity and the total water porosity (Table 3). Taking the ratio of IL-porosity to water porosity yields the IL water as a fraction of the total water content (assuming completely water-saturated clay). This way of expressing water volumes is consistent with the terminology used here in our discussion of the NMR results. Needless to say, an NMR

experiment designed to measure the amount of a certain water phase in a sample should give an  $M_0$  value that is positively correlated with the amount of the corresponding water phase. This idea was utilized in Fig. 4 where the IL water volumes determined by SAXS are plotted vs. the  $M_0$  values associated with short  $T_{1\rho}$  values (in Table 1). Ideally, if the chosen  $M_0$  value is a proper tool for quantifying the IL water volume, then the data points relating the IL water volumes with the corresponding  $M_0$  values should lie on the solid line shown in Fig. 4. Each sample is characterized by one  $M_0$  value associated with a shorter  $T_{1\rho}$  value and another  $M_0$  value associated with a longer  $T_{1\rho}$  value (Table 1). Every sample is thus represented by two data points in the diagram. It is clearly seen that only those data coupled to the shorter  $T_{1\rho}$  values correlate positively with the IL water volume determined by SAXS. Although the above reasoning is not a conclusive proof *sensu stricto*, the combined use of data from the NMR and SAXS measurements strongly supports the interpretation used in this paper, namely that the IL water content is quantitatively given by the  $M_0$  magnetization vector associated with the shorter  $T_{1\rho}$  relaxation time and *vice versa*; the non-IL water content is quantitatively given by the  $M_0$  magnetization vector associated with the longer  $T_{1\rho}$  relaxation time.

One major drawback in the NMR measurements is that the equilibrium cells do not permit real *in situ* measurements; analyses were performed after

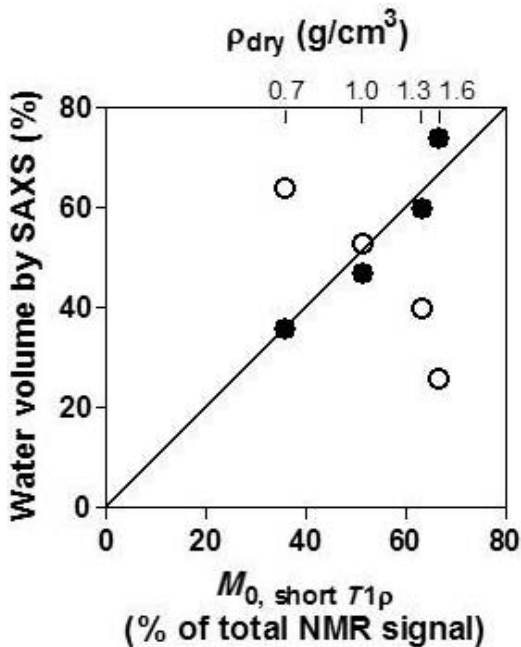


FIG. 4. Relative volumes of IL and non-IL water (in % of total water content) determined by SAXS vs. the magnetization  $M_0$  vector associated with short  $T_{1\rho}$  relaxation times determined by NMR. Filled and open circles refer to the relative volumes of IL and non-IL water, as determined by SAXS.

removing the samples and sub-sampling them. This means that the sample might change somewhat when removed from the cell and that the measured data do not necessarily reflect exactly the same micro-structure as in the constrained conditions encountered in the cell. However, the transfer of each sample from the cell to the NMR tube occurred quickly under normal air and did not alter the soil/water mass ratio.

The possible structural disturbances caused by transferring the samples from the equilibrium cell to the sample tube were studied experimentally. The tests were made on two samples consisting of water-saturated MX-80 mixed with Milli-Q water and compacted to dry densities of 1.3 and 1.6 g/cm<sup>3</sup>. The series also contained one Na montmorillonite sample with a dry density of 1.3 g/cm<sup>3</sup>. The compaction differed slightly from the previous description in that a 9.5 mm long Teflon tube was placed upright in the squeezing cell. The Teflon tube and the rest of the squeezing cell were filled with MX-80/water or montmorillon-

ite/water mixture in such a way that the dry density of the material inside the Teflon tube was the same as in the clay material surrounding it. After compaction to a height of 9.5 mm the sample was taken from the squeezing cell and placed in the equilibrium cell (Fig. 2), where each end of the Teflon tube was in contact with a sinter. The equilibrium cells were disassembled after four weeks and two samples were taken from each cell. One sample was transferred to an NMR glass tube as described previously, thus being exposed to the risk of having its micro-structure disturbed. The sample in the Teflon tube was kept untouched when the tube was removed. Possible disturbances were therefore expected to be less pronounced. The possibility of vertical expansion along the tube could not, however, be ruled out once the sinters were removed. However, no signs of vertical expansion could be seen on inspection by the naked eye. The sample tubes were sealed directly after removal from the equilibrium cell, and stored at room temperature until subsequent  $T_{1\rho}$  measurement in the NMR spectrometer. The results from the few pre-tests did not reveal any difference between the samples that had been stored in the Teflon tubes and those that had been transferred to glass tubes, which was taken as an indication that the transfer of samples from the equilibrium cell to the NMR tube did not, after all, have any significant effect on the micro-structure of the samples. However, in order to rule out the possibility of disturbing the clay microstructure, future studies of this type should be directed towards *in situ* measurements.

### SAXS results

The chemical compositions of the solutions in the external vessels of the SAXS experiment are presented in Table 2. Sodium and chloride are still the most abundant components in the solutions. Most important changes concern sulfate and bicarbonate, which emanate from dissolution of calcite and gypsum.

The data sets of the SAXS measurements on the bentonite samples at two different detector distances were joined together by scaling the low- $q$  data set to coincide with the high- $q$  data set in the overlap region. The scattering intensity  $I(q)$  values are presented for the samples of different density as a function of  $q$  in Fig. 5. The intensities have been vertically shifted in order to get the curves

TABLE 2. Chemical composition of the external solutions at the end of the equilibration.

Sample	Density g/cm <sup>3</sup>	pH	HCO <sub>3</sub> <sup>-</sup> (mM)	Na (mM)	K (mM)	Ca (mM)	Mg (mM)	Cl (mM)	SO <sub>4</sub> (mM)
MX10	0.69	8.08	4.43	105.3	0.79	1.85	0.86	97.6	5.00
MX11	0.99	7.82	4.98	104.8	0.77	1.50	0.74	97.9	4.79
MX12	1.25	8.15	1.95	102.7	0.72	1.20	0.53	98.7	5.10
MX13	1.56	8.15	1.66	106.6	0.56	1.12	0.58	100.1	4.79

separated from each other in the figure. Characteristic of all the curves is the strong peak at about  $q = 0.3\text{--}0.4 \text{ \AA}^{-1}$ . The peak represents the interlayer basal distances of the montmorillonite. The place and shape of the peak depends on the density of the clay, indicating which basal distances are dominant. The MX-80 sample with a dry density of  $0.7 \text{ g/cm}^3$  shows a broad peak also at  $q$  of about  $0.1\text{--}0.2 \text{ \AA}^{-1}$ . At low  $q$  values the SAXS curves approach on log-log scale a straight line with a slope close to  $-3$ . The slope  $-3$  represents the large three-dimensional structures.

The interpretation of the SAXS data obtained in this study was made on the basis of Bragg's law, which thus may add some uncertainty to the reported IL distances. The use of profile modelling will probably improve this in our future work. However, overall trends, like the dependence of the amount of IL water on the dry density, are expected

to be less sensitive to the above uncertainty and, consequently, seem to be basically correct.

In order to obtain a more precise picture of the scattering effects at high  $q$  values the intensity values in Fig. 5 have been modified by dividing them by  $q^s$ , where  $s$  is the exponent of the trend line equation of the linear part of the curves in Fig. 5. Figure 5 presents a fitting curve equation to  $I(q)$  at low  $q$  values for the density of  $0.7 \text{ g/cm}^3$  as an example. The modified intensities are presented in Fig. 6. In the figures the  $x$  axis has been changed from  $q$  for the basal distance, too. The vertical lines in the figures indicate the theoretical basal distances of different bentonite densities assuming a homogeneous structure. In addition to the peaks which represent the IL basal distances in the montmorillonite stacks, there is lower intensity in somewhat larger distances ( $1.8\text{--}8 \text{ nm}$ ). The intensity of those areas depends on the density of the sample such that the

TABLE 3. Modelling of the microstructure in MX-80 samples on the basis of SAXS and chloride exclusion measurements. Layer model is used for the bentonite microstructure.

<b>Input data:</b>					
Dry density (g/cm <sup>3</sup> )		0.7	1.0	1.3	1.6
Water porosity (measured)		0.75	0.64	0.53	0.42
Cl-porosity (measured)		0.37	0.22	0.09	0.05
Theoretical basal distance (Å)		44.4	30.4	22.8	18.1
Basal distance of the main peak (Å)		18.9	18.8	18.2	15.3
Layers per stack (adjusted)		15	18	24	58
Total surface area (m <sup>2</sup> /g)		610	610	610	610
<b>Modelling results:</b>					
IL surface area (m <sup>2</sup> /g)		569	576	584	599
Non-IL surface area (m <sup>2</sup> /g)		41	34	26	11
IL-porosity (volume fraction)		0.27	0.30	0.32	0.31
Non-IL porosity (volume fraction)		0.48	0.34	0.21	0.11
Total Cl-porosity (volume fraction)		0.37	0.22	0.11	0.05
Pore size of non-IL pores (Å)		336	201	124	121

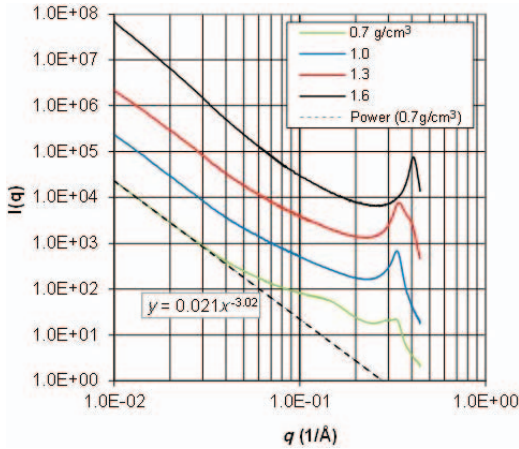


FIG. 5. The intensity as a function of the scattering vector  $q$  for MX-80 samples of different density (in the legend). The intensities have been vertically shifted in order to separate them in the figure. A fitting curve to  $I(q)$  at low  $q$  values is shown for the density  $0.7 \text{ g/cm}^3$ .

intensity is highest at low density and decreases when the density increases. The theoretical basal distances of the homogeneous bentonite are in the area of 1.8–5 nm, and it can be assumed that the measured intensities there represent the most swollen parts of the montmorillonite and possibly the faults (Cebula *et al.*, 1979). The IL distances measured with SAXS given by the main peaks in Fig. 5 were clearly smaller than the theoretical ones assuming

homogenous bentonite, which indicate qualitatively that all water is not in the IL space and that there is also non-IL water.

The SAXS curves were used for evaluation of the IL water amounts in the bentonite samples. In principle, the amount of IL water can be calculated from equation 9 if the IL surface area ( $S_{IL}$ ) and the thickness of the water layer ( $t_{av}$ ) in the IL space are known. The value of  $t$  is obtained from SAXS measurements.  $S_{IL}$  has to be evaluated by some method or used as a fitting parameter. If the thickness of the IL water layer varies, the contributions of different sizes have to be summarized and the  $V_{IL}$  is obtained from equation 10, where  $x_i$  is a weight fraction of bentonite having an IL distance  $t_i$ . The modified intensities in Fig. 6 were used to evaluate the fractions having a certain basal distance. Our assumption is that, in addition to the main peaks, there are larger basal distances and the modified SAXS curves in Fig. 6 represent the distribution of the basal distances. The fraction  $x_i = C_i/C$ , where  $C_i$  is the intensity at a certain basal distance and  $C$  is the sum of the intensities over the observed area. The IL water can then be calculated from equation 11.;

$$V_{IL} = \frac{1}{2} S_{IL} t_{av} \tag{9}$$

$$V_{IL} = \frac{1}{2} \sum x_i S_{IL} t_i \tag{10}$$

$$V_{IL} = \frac{1}{2} \sum \frac{C_i}{C} S_{IL} t_i \tag{11}$$

Separating of the overlapping peaks representing each number of molecular layers of water in the

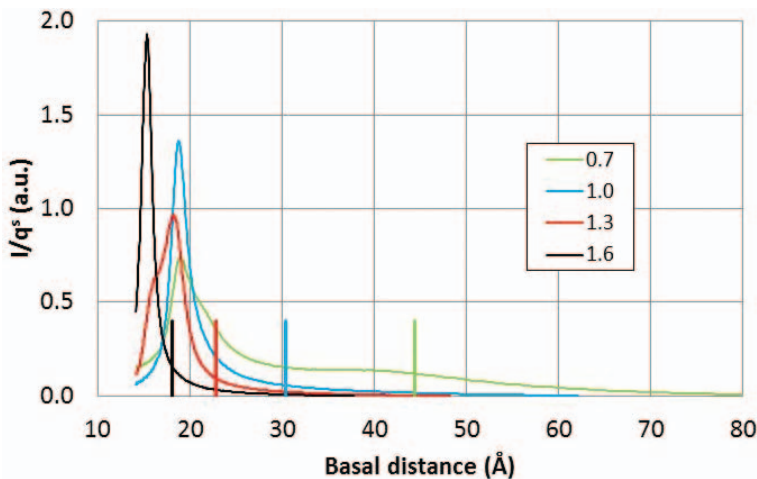


FIG. 6. The modified intensity as a function of the basal distance for MX-80 samples of different dry density seen in the legend. The theoretical basal distances of the homogeneous samples are indicated with the vertical lines of the same colours on the x-axes.

interlayer space is challenging due to the strong overlapping of the peaks at higher basal distance values. A simplified method is to allow each  $q$  value (channel of counts) to represent an interlayer distance and the counts to represent the fraction of montmorillonite having this interlayer distance. In this way, the interlayer distances will be considered over the whole area in water amount calculations, although the exact contributions of the different water layer numbers are not specified. The chloride porosity measurements and Donnan exclusion calculations were used together with the SAXS results to evaluate the bentonite microstructure. The bentonite structure used in the evaluation was of the same type as described earlier in many publications (Wersin, 2003; Suzuki *et al.*, 2004; Muurinen *et al.*, 2007; Tournassat & Appello, 2011), where the montmorillonite is organized in stacks having IL water between the layers and non-IL water between the stacks.

The chloride porosity  $\varepsilon_{Cl}$  was evaluated from the volume-based concentration ratios between the bentonite and the external solution from equation 12, where  $m_{Cl}$  is the mass of chloride in the studied bentonite sample,  $m_b$  is the dry mass of bentonite,  $\rho_g$  is the grain density of bentonite (2.75 g/cm<sup>3</sup>),  $V_w$  is the volume of water in the water-saturated bentonite sample, and  $C_{Cl}^0$  is the chloride concentration in the external solution.

$$\varepsilon_{Cl} = \frac{m_{Cl}}{(m_b/\rho_g + V_w)C_{Cl}^0} \quad (12)$$

The water contents measured for the MX-80 samples taken 1–3 mm from the water bentonite interface gave somewhat lower densities than aimed for in the case of the samples 1.3 g/cm<sup>3</sup> (measured 1.25 g/cm<sup>3</sup>) and 1.6 g/cm<sup>3</sup> (measured 1.55 g/cm<sup>3</sup>). It is possible that there was a density gradient in the sample which caused this difference. In the calculations performed on the SAXS samples taken further from the filter plate, the planned densities were used instead of the values calculated from the water content measurements.

According to the Donnan model, polyelectrolytes, like bentonite, in contact with salt solutions through a membrane are expected to have a unique content of ions in the porewater. Equation 13, which is based on the Donnan model, presents the relationship between the concentration of a monovalent cation in the external water and porewater (Overbeek, 1952; Karnland, 1998; Ståhlberg, 1999)

$$\gamma_{ie}C_{ie} = \frac{1}{2} \left[ -\gamma_{cc}C_{cc} + \sqrt{\gamma_{cc}^2C_{cc}^2 + 4\gamma_e^sC_e^2} \right] \quad (13)$$

where  $C_e$  is the cation concentration in the external water (mol/l),  $C_{ie}$  is the cation concentration caused by the external water into the porewater (mol/l),  $C_{cc}$  is the concentration caused by the exchangeable cations into the porewater (mol/l), and  $\gamma_{ie}$ ,  $\gamma_{cc}$  and  $\gamma_e$  are activity coefficients in different conditions.

$C_{cc}$  can be evaluated from the cation-exchange capacity and water content in the clay. In the case where chloride and sodium are the only ions in the system, the chloride concentration in the porewater is equal to  $C_{ie}$ . By assuming that all the activity coefficients are equal, the concentration caused by the external solution into the porewater can be solved.

Donnan exclusion modelling was done for the MX-80 samples assuming a homogeneous or dual porosity structure in the montmorillonite. The total surface area of the bentonite used in the calculations was 610 m<sup>2</sup>/g, CEC was 84 meq/g (Kumpulainen & Kiviranta, 2010, 2011) and the grain density 2.75 g/cm<sup>3</sup>. The concentration caused by the exchangeable cations in the porewater ( $C_{cc}$ ) could then be calculated. The cation concentration caused by the external solution into the porewater ( $C_{ie}$ ) was solved from equation 13 and the chloride porosity from equation 12. The effect of the dissolving accessory minerals (gypsum, calcite) was ignored in the modelling. In the model with the dual porosity, the fraction of the montmorillonite of each basal distance was calculated from equation 11 using the curve of the modified intensity vs. the basal distance in Fig. 6. This allows calculation of the total water amount in the interlayer space when the surface area of montmorillonite seen by SAXS is known. However, it is not possible to conclude from the SAXS curve which fraction of montmorillonite contributes to the SAXS spectra, i.e. which part of the surface area can be considered as an interlayer one. In the modelling, the number of layers in the stacks was used as a fitting parameter. It was adjusted so that the modelled chloride concentration was equal to the measured value. Chloride was allowed to go both to the IL and non-IL water according to the Donnan model. In the calculations, the interlayer size was allowed to extend to twice the theoretical homogeneous basal distance. The input data used in the modelling and the obtained results of MX-80 bentonite are presented in Table 3.

The results from the NMR measurements and SAXS measurements are compared in Fig. 7. The figures present IL, non-IL, water and chloride porosity in MX-80 samples saturated with 0.1 M NaCl solution at different dry densities. The NMR studies and SAXS studies coupled with the Cl exclusion modelling provide very similar pictures of how the porewater is divided into two phases in bentonite. The trend lines of the IL and non-IL porosity seen in the figure were calculated from the SAXS and NMR results together. The second-order regression equations presented in the figure caption describe well the porosities as a function of the dry density of bentonite within the described density area. The diagrams also show that the chloride porosity is smaller than the non-IL porosity indicating the exclusion. The Donnan modelling based on the homogeneous montmorillonite in bentonite (Fig. 7) gives clearly lower Cl-porosity than the measured one.

The subsamples for SAXS and NMR measurements had to be cut from the larger bentonite sample of the experiment. For this purpose the initially confined bentonite has to be opened and the swelling pressure released. How much this

changes the sample is not clear at the moment. The above clearly underline the need for performing *in situ* experiments. Excellent examples of *in situ* experiments are the neutron-scattering measurements on compacted water-saturated bentonite performed by Devineaux *et al.* (2006).

Uncertainties are related to the Donnan model used for evaluation of the chloride exclusions, too. According to Tournassat & Appelo (2012) the model is more suitable for the high-density conditions than for the low density conditions. The difficulty of taking into account the divalent ions and the evaluation of the activity coefficients brings more uncertainty to the result. The use of chloride exclusion for the evaluation of the IL and non-IL surface areas is not needed when the SAXS and NMR samples are taken from the same experiment. Then the surface areas can be calculated directly from SAXS and NMR data without the exclusion calculations.

## SUMMARY AND CONCLUSIONS

Knowledge about the microstructure of the bentonite and the distribution of water between different

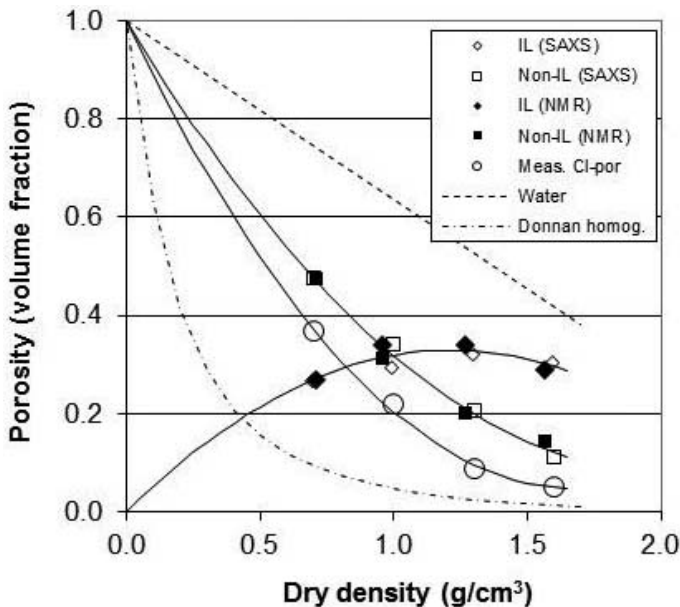


FIG. 7. IL and non-IL porosity evaluated from SAXS and NMR measurements, measured chloride porosity, water porosity and Donnan modelling of Cl-porosity in homogeneous MX-80 bentonite saturated with 0.1 M NaCl solution at different dry density. The trend lines are IL:  $y = -0.2231x^2 + 0.541x$ ;  $R^2 = 0.981$ , non-IL:  $y = 0.223x^2 - 0.905x + 1$ ;  $R^2 = 0.997$ , Cl porosity:  $y = 0.337x^2 - 1.133x + 1$ ;  $R^2 = 0.999$ .

pore types is useful to model long-term processes in the bentonite in an HLW repository. The porosity is often considered to be divided into two distinguishable parts, interlayer (IL) and non-interlayer (non-IL) pores. The water in these pores is generally assumed to have different properties as a consequence of how much it is influenced by the electric fields emanating from the negatively charged montmorillonite unit layers. Close to the basal unit layer surfaces, the anions are affected by the negative surface, which is the reason why anion exclusion occurs. It is thus possible to sub-divide the non-IL water to smaller categories, like “diffuse double-layer water” and “free water”. In the present study, however, the result was explained in terms of the IL and non-IL concepts and no further sub-division of the water phases was used.

The research on water-saturated clay microstructure benefits from combining techniques to get complementary data. In the present study, NMR, SAXS and chloride exclusion were used for this purpose. The present study was carried out with MX-80 bentonite. The sample dry densities ranged between 0.7 and 1.6 g/cm<sup>3</sup>. The NMR results were obtained by using <sup>1</sup>H NMR  $T_{1\rho}$  relaxation time measurements using the short inter-pulse CPMG method. The interpretation of the NMR results was based on the fitting of discrete exponentials to the observed decay curves. The results by NMR indicated for compacted samples the presence of two main types of water, which were interpreted as IL and non-IL water.

The SAXS measurement on bentonite samples were used to get information about the size distribution of the IL distance of montmorillonite. The IL distances measured with SAXS were clearly smaller than the theoretical ones assuming homogeneous bentonite, which indicated qualitatively that all water was not in the IL space and there is also non-IL water. The chloride porosity measurements and Donnan exclusion calculations were used together with the SAXS results to evaluate the bentonite microstructure. The layer model, where the montmorillonite was organized in stacks having IL water between the layers and non-IL water between the stacks, was used in the evaluation. In the modelling, the number of layers in the stacks was used as fitting parameters which determined the IL and non-IL surface areas. The fitting parameters were adjusted so that the modelled chloride concentration was equal to the measured one.

The studies carried out with two different methods, NMR and SAXS studies coupled with Cl porosity measurements, provided very similar pictures of how the porewater is divided in IL and non-IL water in the bentonite. The IL and non-IL porosities of this study were in most cases in line with the porosities found in the literature. The only exception was the clearly lower values of non-IL porosity presented by Holmboe *et al.* (2012). In that study it was obviously assumed that the clay was homogeneous, no stacking occurred, and that the total surface area was identical with the whole IL surface area. These assumptions lead to the exceptionally high IL water and low non-IL water values presented by Holmboe *et al.* It is probable, however, that the real situation in the bentonite is more complex than the used microstructural model in this study where the non-IL pores were assumed to be of the same size. More realistic modelling would, however, need data about the non-IL pore size distributions, which is not available at the moment.

#### ACKNOWLEDGMENTS

The work was funded by Posiva Oy. The SAXS measurements were carried out by Panu Hiekkataipale at The Nanomicroscopy Center of Aalto University.

#### REFERENCES

- Birgersson M. & Karnland O. (2009) Ion equilibrium between montmorillonite interlayer space and the external solution. *Geochimica et Cosmochimica Acta*, **73**, 1908–1923.
- Bolt G. & De Haan F. (1982) *Soil Chemistry B. Physico-Chemical Models*. Elsevier, Amsterdam/New York.
- Bolt G. & Warkentin B. (1958) The negative adsorption of anions by clay suspensions. *Kolloid Zeitschrift*, **156**, 41–46.
- Bradbury M.H. & Baeyens B. (2003) Porewater chemistry in compacted re-saturated MX-80 bentonite. *Journal of Contaminant Hydrology*, **61**, 329–338.
- Carlsson T., Muurinen A., Matuszewicz M. & Root A. (2012) Porewater in compacted water-saturated MX-80 bentonite. Pp. 397–402 in: *Materials Research Society Symposium Proceedings*, **1475** (R.M. Carranza, G.S. Duffó & R.B. Rebak, editors). Materials Research Society, Warrendale, Pennsylvania.
- Cebula D.J., Thomas R.K. & White J.W. (1979) The structure and dynamics of clay-water systems studied

- by neutron scattering. *Developments in Sedimentology*, **27**, 111–120.
- Devineau K., Bihannic I., Michot L., Villieras F., Masroui F., Cuisinier O., Fragneto G. & Michau N. (2006) In situ neutron diffraction analysis of the influence of geometric confinement on crystalline swelling of montmorillonite. *Applied Clay Science*, **31**, 76–84.
- Edwards D. & Quirk J. (1962) Repulsion of chloride by montmorillonite. *Journal of Colloid Science*, **17**, 872–882.
- Eriksen T. & Jacobsson A. (1984) Diffusion in clay. Experimental techniques and theoretical models. *KBS Technical Report*, **84–05**, Swedish Nuclear Fuel Supply Co., Stockholm, Sweden.
- Farrar T.C. & Becker E.D. (1971) *Pulse and Fourier Transform NMR: Introduction to Theory and Methods*. Academic Press, New York.
- Fernández A.M. & Rivas P. (2005) Analysis and distribution of waters in the compacted FEBEX bentonite: pore water chemistry and adsorbed water. Pp. 257–275 in: *Advances in Understanding Engineered Clay Barriers* (E.E. Alonso & A. Ledesma, editors). Taylor & Francis Group, London.
- Ferrage E., Tournassat C., Rinnert E. & Lanson B. (2005) Influence of pH on the interlayer cationic composition and hydration state of Ca-montmorillonite: Analytical chemistry, chemical modelling and XRD profile modelling study. *Geochimica et Cosmochimica Acta*, **69**, 2797–2812.
- Holmboe M. (2011) *The Bentonite Barrier: Microstructural properties and the influence of  $\gamma$ -radiation*. PhD thesis, Royal Institute of Technology, Stockholm.
- Holmboe M., Wold S. & Jonsson M. (2012). Porosity investigation of compacted bentonite using XRD profile modelling. *Journal of Contaminant Hydrology* **128**, 19–32.
- Karlund O. (1998) Bentonite swelling pressure in strong NaCl solutions. *POSIVA Report*, **98–01**, Posiva Oy, Helsinki.
- Karlund O., Muurinen A. & Karlsson F. (2005) Bentonite swelling pressure in NaCl solutions – Experimentally determined data and model calculations. Pp. 241–256 in: *Advances in Understanding Engineered Clay Barriers* (E.E. Alonso & A. Ledesma, editors). Taylor & Francis Group, London.
- Karlund O., Olsson S. & Nilsson U. (2006) Mineralogy and sealing properties of various bentonites and smectite-rich clay materials. *KBS Technical Report*, **06–30**, Swedish Nuclear Fuel and Waste Management Co., Stockholm.
- Kaufhold S., Dohrmann R., & Klinkenberg M. (2010) Water-uptake capacity of bentonites. *Clays and Clay Minerals*, **58**, 37–43.
- Kozaki T., Inada K., Sato S. & Ohashi H. (2001) Diffusion mechanisms of chloride in sodium montmorillonite. *Journal of Contaminant Hydrology*, **47**, 159–170.
- Kristukat C. (2008) *Peak-o-mat*. [https://sourceforge.net/project/showfiles.php?group\\_id=67624](https://sourceforge.net/project/showfiles.php?group_id=67624).
- Kumpulainen S. & Kiviranta L. (2010) Mineralogical and Chemical Characterization of Various Bentonite and Smectite-Rich Clay Materials. *POSIVA Working Report*, **2010–52**, Posiva Oy, Olkiluoto.
- Kumpulainen S. & Kiviranta L. (2011) Mineralogical, Chemical and Physical Study of Potential Buffer and Backfill Materials from ABM Test Package 1. *POSIVA Working Report*, **2011–41**, Posiva Oy, Olkiluoto.
- Moleira M., Eriksen T. & Jansson M. (2003) Anion diffusion pathways in bentonite clay compacted to different dry densities. *Applied Clay Science*, **23**, 69–76.
- Montavon G., Guo Z., Tournassat C., Grambow B. & Le Botlan D. (2009) Porosities accessible to HTO and iodide on water-saturated compacted clay materials and relation with the forms of water: A low field proton NMR study. *Geochimica et Cosmochimica Acta*, **73**, 7290–7302.
- Morvan M., Espinat D., Lambard J. & Zemb Th. (1994) Ultrasmall- and small-angle X-ray scattering of smectite clay suspensions. *Colloids and Surfaces A: Physicochemical and Engineering Aspects*, **82**, 193–203.
- Muurinen A. (1994) *Diffusion of Anions and Cations in Compacted Sodium Bentonite*. VTT Publications 168, Technical Research Centre of Finland Espoo.
- Muurinen A. (2009) Studies on the Chemical Conditions and Microstructure in the Reference Bentonites of Alternative Buffer Materials Project (ABM) in Äspö. *POSIVA Working Report*, **2009-42**, Posiva Oy, Olkiluoto.
- Muurinen A. & Carlsson T. (2010) Experiences of pH and Eh measurements in compacted MX-80 bentonite. *Applied Clay Science*, **47**, 23–27.
- Muurinen A. & Carlsson T. (2013) Bentonite pore structure based on SAXS, chloride exclusion and NMR studies. *POSIVA Report* (to be published).
- Muurinen A, Karlund O. & Lehtikoinen J. (2007) Effect of homogenization on the microstructure and exclusion of chloride in compacted bentonite. *Physics and Chemistry of the Earth, Parts A/B/C*, **32**, 485–490.
- Ohkubo T., Kikuchi H. & Yamaguchi M. (2008) An approach of NMR relaxometry for understanding water in saturated compacted bentonite. *Physics and Chemistry of the Earth*, **33**, S169–S176.
- Overbeek J. (1952) Electrochemistry of the double layer. Pp. 115–193 in: *Colloid Science* (H. Kruyt, editor). Elsevier Publishing Company, Amsterdam.
- Pusch R. (1999) Microstructural evolution of buffers. *Engineering Geology*, **54**, 33–41.
- Pusch R., Karlund O. & Hökmark H. (1990) GMM – a general microstructural model for qualitative and

- quantitative studies on smectite clays. *KBS Technical Report*, **90–43**, Swedish Nuclear Fuel and Waste Management Co., Stockholm.
- Santyr G.E., Henkelman R.M. & Bronskill M.J. (1988) Variation in measured transverse relaxation in tissue resulting from spin locking with the CPMG sequence. *Journal of Magnetic Resonance*, **79**, 28–44.
- Segad M., Jönsson B., Åkesson T. & Cabane B. (2010) Ca/Na montmorillonite: Structure, forces and swelling properties. *Langmuir*, **26**, 5782–5790.
- Sposito G. (1982) The diffuse-ion swarm near smectite particles suspended in 1:1 electrolyte solutions: modified Gouy-Chapman theory and quasicrystal formation. Pp. 127–156 in: *Clay-Water Interface and its Rheological Implications* (N. Güven & R.M. Pollastro, editors). Clay Minerals Society.
- Ståhlberg J. (1999) Retention model for ions in chromatography. *Journal of Chromatography A*, **855**, 3–55.
- Suzuki S., Sato H., Ishidera T. & Fujii N. (2004) Study on anisotropy of effective diffusion coefficient and activation energy for deuterated water in compacted sodium bentonite. *Journal of Contaminant Hydrology*, **68**, 23–37.
- Tertre E., Prêt D & Ferrage E. (2011a) Influence of the ionic strength and solid/solution ratio on Ca(II)-for-Na<sup>+</sup> exchange on montmorillonite. Part 1: Chemical measurements, thermodynamic modelling and potential implications for trace elements geochemistry. *Journal of Colloid and Interface Science*, **353**, 248–256.
- Tertre E., Ferrage E., Bihannic I., Michot L.J. & Prêt D. (2011b) Influence of the ionic strength and solid/solution ratio on Ca(II)-for-Na<sup>+</sup> exchange on montmorillonite. Part 2: Understanding the effect of the *m/V* ratio. Implications for pore water composition and element transport in natural media. *Journal of Colloid and Interface Science*, **363**, 334–347.
- Tournassat C. & Appelo C.A.J. (2011). Modelling approaches for anion-exclusion in compacted Na-bentonite. *Geochimica et Cosmochimica Acta*, **75**, 3698–3710.
- Van Loon L.R., Glaus M.A. & Müller W. (2007) Anion exclusion effects in compacted bentonites: towards a better understanding of anion diffusion. *Applied Geochemistry*, **22**, 2536–2552.
- van Olphen H. (1977) *An Introduction to Clay Colloid Chemistry*. John Wiley & Sons, New York.
- Warr L. & Berger J. (2007) Hydration of bentonite in natural waters: Application of “confined volume” wet-cell X-ray diffractometry. *Physics and Chemistry of the Earth*, **32**, 247–258.
- Wersin P. (2003) Geochemical modelling of bentonite porewater in high-level waste repositories. *Journal of Contaminant Hydrology*, **61**, 405–422.